Co-published by
Institute of Fluid-Flow Machinery
Polish Academy of Sciences
Committee on Thermodynamics and Combustion
Polish Academy of Sciences

Copyright©2024 by the Authors under licence CC BY-NC-ND 4.0

http://www.imp.gda.pl/archives-of-thermodynamics/

Analysis of unsteady heat and mass transfer in rotating MHD convection flow over a porous vertical plate

Mohanasundaram Narmatha[a], R. Kavitha[b*],

[a]Department of Mathematics, KPR Institute of Engineering and Technology, Coimbatore, India
[b]Department of Mathematics and Statistics, Faculty of Science and Humanities, SRM Institute of Science and Technology, Chengalpattu, India
*Corresponding author email: kavibalki13@gmail.com

Received: 24.11.2023; revised: 12.07.2024; accepted: 30.09.2024

Abstract

The aim of this research paper is to investigate the rotational flow of an unsteady magnetohydrodynamic heat and mass transfer flow due to convection over a vertical porous semi-infinite plate. The plate undergoes continuous circular motion, maintaining a constant velocity. To achieve this, we worked on both numerical methods and analytical techniques, particularly utilizing perturbation methods to solve the governing partial differential equations. Consequently, we derive an expression for the Nusselt and Sherwood numbers. We delve into the analysis of the velocity profile, temperature distribution, and concentration variation, exploring their behaviour under different physical parameters, including the magnetic field parameter, Grashof number, Soret number and Schmidt number, as well as the Prandtl number. Our findings reveal that the velocity increases with rising values of Grashof, modified Grashof and Soret numbers, whereas it decreases with declining values of the magnetic field parameter, Prandtl number and Schmidt number. Additionally, as rotation gradually intensifies, the fluid velocity closely follows the boundary and becomes negligible as it moves away from it. To facilitate a comprehensive examination of the fluid flow and heat and mass transfer characteristics, we employ graphical representations. Furthermore, this paper offers an in-depth discussion of the underlying physical aspects and their implications.

Keywords: Heat transfer; Magnetohydrodynamics; Mass transfer; Rotation; Soret number; Perturbation law; Porous plate; Heat source

Vol. 45(2024), No. 4, 179–187; doi: 10.24425/ather.2024.152007

Cite this manuscript as: Narmatha, M., & Kavitha, R. (2024). Analysis of unsteady heat and mass transfer in rotating MHD convection flow over a porous vertical plate. *Archives of Thermodynamics*, 45(4), 179−187.

1. Introduction

Combined heat and mass transfer (HMT) plays a crucial role in various engineering applications. Recent research suggests that mass transfer (MT) can potentially reduce heat transfer (HT) in high-speed vehicles like aircraft and missiles, making it an attractive area of exploration. Rotating flows are fundamental to numerous scientific and engineering fields. From designing jet engines, pumps and vacuum cleaners to understanding geophysical phenomena, the analysis of rotating incompressible fluids holds significant importance. Its applications even extend to space science and engineering thermodynamics.

This research builds upon existing studies such as Chamkha et al. [1] investigations of magnetohydrodynamic (MHD) flow with hall current, and Mohyud Din et al. [2] work on nanofluids using Buongiorno's model. Both employed numerical methods for their analyses. Furthermore, Kataria and Patel's [3] research explored the influence of oscillating plates in Casson fluid flow.

Nomenclature

A –velocity ratio parameter
B_0 – magnetic induction, T
C_p – specific heat, J/(kg K)
C_w*– dimensional wall concentration, kg/m^3
C* – dimensional concentration, kg/m^3
C_∞ – ambient concentration, kg/m^3
D_M – coefficient of chemical molecular diffusivity, m^2/s
D_T – coefficient of thermal diffusivity, m^2/s
g – gravitational acceleration, m/s^2
Gm– modified Grashoff number
Gr – Grashoff number
k – thermal conductivity, W/(m K)
K – permeability, m^2
K* – mean absorption coefficient, m^{-1}
M – magnetic field parameter
n* – arbitrary constants
N – components of microrotation
Nu – Nusselt number
Pr – Prandtl number
q_r – radiative heat flux, W/m^2
q_W – the rate of heat transfer, W/m^2
Q – heat source, W/m^3
R – thermal radiation, W/m^2
Re$_x$ – local Reynold number
Sc – Schmidt number
Sh – Sherwood number
So – Soret number
t – time, s
T* – dimensional temperature, K
T_w*– dimensional wall temperature, K
T_∞ – ambient temperature, K
u, v – non-dimensional components of velocity
u^*, v^*– components of velocity, m/s
U_0, V_0– arbitrary constants, m/s
U_∞ – free stream velocity, m/s
x, y – Cartesian coordinates, m

Greek symbols

β – coefficient of thermal expansion
β^* – coefficient of concentration expansion
ε – factor of higher order
ϑ – non-dimensional temperature
μ – dynamic viscosity, Pa·s
ρ – density, kg/m^3
ρ_∞ – ambient density, kg/m^3
σ – electrical conductivity, S/m
σ* – Stefan-Boltzmann constant, W/(m^{2}K^4)
τ – shear stress, Pa
υ – kinematic viscosity, m^2/s
Ω – angular velocity, rad/s

Abbreviations and Acronyms

PDEs– partial differential equations
HMT – heat and mass transfer
HT – heat transfer
MHD– magnetohydrodynamic
MT – mass transfer

Subscripts

w – condition at the surface
∞ – condition at the free stream

The significance of MHD (magnetohydrodynamics) extends beyond theoretical aspects. Engineers utilize MHD principles in heat exchanger design, compressors and spacecraft power systems. Additionally, MHD finds application in separating molten materials and developing novel power generation methods. These diverse applications highlight the necessity of investigating problems involving MHD effects.

Existing literature highlights the importance of studying rotational and MHD effects in fluid flow. Several studies by Seth et al [4,5], Shevchuk [6], Takhar et al., [7], and Jha and Apere [8] have explored these areas in various contexts, including rotating convective flow, MHD on rotating disks and MHD flow between parallel plates. MHD effects near porous media have also been investigated by Abdel Rahman [9], while research on unsteady rotating flows was carried out by Veera Krishna et al. [10], which provides insights into drag experiences in specific geometries. Ahmmed et al. [11] examined the MHD unsteady flow with a heat source engrossed in a porous medium. Seddeek [12] investigated MHD's unsteady thermal convective flow past a semi-infinite flat plate. Furthermore, the performance of a centrifugal compressor fitted with a rotating tapered vaneless diffuser was investigated by Niveditha and Prasad [13] using the numerical ANSYS CFX software. Combined effects of rotation and other factors were studied by Narayanan et al. [14] and Rudziva et al. [15].

Motivated by the gap in Ahmmed et al.'s work [11] which lacked a combined analysis of MHD unsteady convection, HMT, and a porous medium, this study aims at: investigating MHD unsteady convective HMT flow past a vertical porous plate, employing both numerical (MATLAB) and analytical (perturbation technique) methods to solve the governing equations; obtaining expressions for the Nusselt and Sherwood numbers; analyzing the characteristics of fluid flow, HMT; and discussing the physical implications through the use of graphs.

2. Mathematical formulation

Consider the 2D unsteady MHD rotating convective HMT flow of an incompressible, viscous fluid past a vertically moving porous plate with a uniform magnetic field. We choose the x*-axis to run vertically along the plate and the y*-axis to run perpendicular to the plate which is shown in Fig. 1. It is assumed that no voltage is applied, implying that no electric field exists. The transverse magnetic field and magnetic Reynolds number are both extremely low. The induced magnetic field is insignificant.

The governing equations are as follows:

$$\frac{\partial v^*}{\partial y^*} = 0, \tag{1}$$

$$\rho\left(\frac{\partial u^*}{\partial t^*} + v^*\frac{\partial u^*}{\partial y^*}\right) = \frac{\partial p^*}{\partial x^*} + \mu\frac{\partial^2 u^*}{\partial y^*} - \rho\beta - \frac{\mu}{K^*}u^* + \\ -\sigma B_0^2 u^* + 2\Omega u^*, \tag{2}$$

$$\frac{\partial T^*}{\partial t^*} + v^* \frac{\partial T^*}{\partial y^*} = \frac{k}{\rho C_p}\frac{\partial^2 T^*}{\partial y^{*2}} - \frac{1}{\rho C_p}\left(\frac{\partial q_r^*}{\partial y^*}\right) - \frac{Q_0}{\rho C_p}(T^* - T_\infty^*), \quad (3)$$

$$\frac{\partial C^*}{\partial t^*} + v^* \frac{\partial C^*}{\partial y^*} = D_M \frac{\partial^2 C^*}{\partial y^{*2}} + D_T \frac{\partial^2 T^*}{\partial y^{*2}}. \quad (4)$$

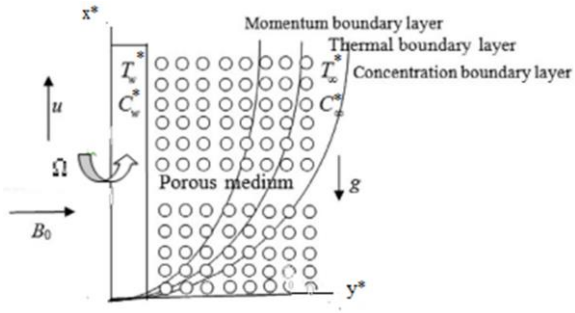

Fig. 1. Physical model.

The boundary conditions are as follows:

– at $y^* = 0$

$$u^* = u_p^*, T^* = T_w^* + \varepsilon(T_w^* - T_\infty^*)e^{n^* t^*}, \quad C^* = C_w^* + \varepsilon(C_w^* - C_\infty^*)e^{n^* t^*}, \quad (5)$$

– at $y^* \to \infty$

$$u^* \to U_\infty^* = U_0\left(1 + \varepsilon e^{n^* t^*}\right), \quad T^* \to T_\infty^*, \quad C^* \to C_\infty^*. \quad (6)$$

From Eq. (1), we deem an exponential form for the velocity:

$$v^* = -v_0(1 + \varepsilon A e^{n^* t^*}), \quad (7)$$

$$\rho\frac{dU_\infty^*}{dt^*} = \frac{\partial p^*}{\partial x^*} - \rho_\infty g - \frac{\mu}{K^*}U_\infty^* - \sigma B_0^2 U_\infty^*, \quad (8)$$

$$\rho\left(\frac{\partial u^*}{\partial t^*} + v^*\frac{\partial u^*}{\partial y^*}\right) = (\rho_\infty - \rho)g + \rho\frac{dU_\infty^*}{dt^*} + \mu\frac{\partial^2 u^*}{\partial y^{*2}} - \frac{\mu}{K^*}(U_\infty^* - u^*) - \sigma B_0^2(U_\infty^* - u^*). \quad (9)$$

Utilizing the equation of state:

$$\frac{(\rho_\infty - \rho)}{\rho_\infty} = \beta\frac{(T^* - T_\infty^*)}{T_\infty^*} + \beta^*\frac{(C^* - C_\infty^*)}{C_\infty^*}, \quad (10)$$

and plugging Eq. (10) into Eq. (9), we have:

$$\frac{\partial u^*}{\partial t^*} + v^*\frac{\partial u^*}{\partial y^*} = \frac{dU_\infty^*}{dt^*} + \mu\frac{\partial^2 u^*}{\partial y^{*2}} + g\beta\frac{(T^* - T_\infty^*)}{T_\infty^*} + g\beta^*\frac{(C^* - C_\infty^*)}{C_\infty^*} + \frac{v}{K^*}(U_\infty^* - u^*) + \frac{\sigma B_0^2}{\rho}(U_\infty^* - u^*). \quad (11)$$

The radiative heat flux term, as expressed using the Rosseland approximation, is given by:

$$q_r^* = \frac{4\sigma^*}{3k_1^*}\frac{\partial {T^*}^4}{\partial y^*}. \quad (12)$$

Within the flow, the temperature difference is considered small, so that ${T^*}^4$ can be expressed as a temperature-dependent linear function. This is achieved by expanding $T_\infty{}^*$ in a Taylor series while ignoring higher-order terms, resulting in:

$${T^*}^4 \cong 4T_\infty^{*3} - 3T_\infty^{*4}. \quad (13)$$

By using Eqs. (12) and (13) in Eq. (3), we get:

$$\frac{\partial T^*}{\partial t^*} + v^*\frac{\partial T^*}{\partial y^*} = \frac{k}{\rho C_p}\frac{\partial^2 T^*}{\partial y^{*2}} - \frac{16\sigma^* T_\infty^{*3}}{3\rho C_p k_1^*}\frac{\partial^2 T^*}{\partial y^{*2}} - \frac{Q_0}{\rho C_p}(T^* - T_\infty^*). \quad (14)$$

2.1. Solution of the problem

Non-dimensional quantities are introduced to find the solution of Eqs. (1) to (4) with boundary conditions (5) and (6):

$$u^* = uU_0, \quad v^* = vV_0, \quad T^* = T_\infty^* + \vartheta(T_w^* - T_\infty^*), \quad C^* = C_\infty^* + C(C_w^* - C_\infty^*), \quad U_\infty^* = U_\infty U_0,$$

$$u_p^* = U_p U_0, \quad K^* = \frac{Kv^2}{V_0^2}, \quad y^* = \frac{yv}{V_0}, \quad \mathrm{Gm} = \frac{vg\beta^*(C_w^* - C_\infty^*)}{V_0^2 U_0 C_\infty^*},$$

$$\mathrm{Gr} = \frac{vg\beta(T_w^* - T_\infty^*)}{V_0^2 U_0 T_\infty^*}, \quad \mathrm{Pr} = \frac{v\rho C_p}{k}, \quad M = \frac{\sigma B_0^2 v}{\rho V_0^2}, \quad Q = \frac{Q_0 v}{\rho V_0^2 C_p},$$

$$R = \frac{4\sigma^* T_\infty^{*3}(T_w^* - T_\infty^*)}{k_1^* k}, \quad \mathrm{Sc} = \frac{v}{D_M}, \quad t^* = \frac{tv}{V_0^2}, \quad n^* = \frac{V_0^2}{v}. \quad (15)$$

As a result, the dimensionless governing equations are expressed by Eqs. (16) to (19) with boundary conditions (20):

$$\frac{\partial v}{\partial y} = 0, \quad (16)$$

$$\frac{\partial u}{\partial t} + v\frac{\partial u}{\partial y} = \frac{dU_\infty}{dt} + \frac{\partial^2 u}{\partial y^2} + \mathrm{Gr}\vartheta + \mathrm{Gm}C + N(U_\infty - u), \quad (17)$$

$$\frac{\partial \vartheta}{\partial t} + v\frac{\partial \vartheta}{\partial y} = \frac{1}{\mathrm{Pr}}\left(1 + \frac{4R}{3}\right)\frac{\partial^2 \vartheta}{\partial y^2} - Q\vartheta, \quad (18)$$

$$\frac{\partial C}{\partial t} + v\frac{\partial C}{\partial y} = \frac{1}{\mathrm{Sc}}\frac{\partial^2 C}{\partial y^2} + \mathrm{So}\frac{\partial^2 \vartheta}{\partial y^2}. \quad (19)$$

The corresponding initial and boundary conditions are:

– at $y = 0$

$$u = U_p, \quad \vartheta = 1 + \varepsilon e^{nt}, \quad C = 1 + \varepsilon e^{nt}, \quad (20)$$

– as $y \to \infty$

$$u \to U_\infty \to 1 + \varepsilon e^{nt}, \quad \vartheta \to 0, \quad C \to 0.$$

We consider the following solutions for the perturbation technique to solve Eqs. (16) to (19):

$$u = u_0(y) + \varepsilon e^{nt}u_1(y) + o(\varepsilon^2), \quad \vartheta = \vartheta_0(y) + \varepsilon e^{nt}\vartheta_1(y) + o(\varepsilon^2), \quad C = C_0(y) + \varepsilon e^{nt}C_1(y) + o(\varepsilon^2). \quad (21)$$

By plugging Eqs. (21) into Eqs. (16)–(20), and then equating the harmonic and non-harmonic terms and ignoring higher order terms of $o(\varepsilon^2)$, we get the following pairs of equations:

$$u_0'' + u_0' + (2\Omega - N)u_0 = -N - \mathrm{Gr}\vartheta_0 - \mathrm{Gm}C_0, \quad (22)$$

$$u_1'' + u_1' - (N + n + 2\Omega)u_1 = -(N + n) - Au_0' - \mathrm{Gr}\vartheta_1 - \mathrm{Gm}C_1, \quad (23)$$

$$(3+4R)\vartheta_0^{''} + 3\mathrm{Pr}\vartheta_0' - 3Q\mathrm{Pr}\vartheta_0 = 0, \quad (24)$$

$$(3+4R)\vartheta_1^{''} + 3\mathrm{Pr}\vartheta_1' - (3n+Q)\mathrm{Pr}\vartheta_1 = -3A\mathrm{Pr}\vartheta_0', \quad (25)$$

$$C_0^{''} + \mathrm{Sc}C_0' = -\mathrm{SoSc}\vartheta_0^{''}, \quad (26)$$

$$C_1^{''} + \mathrm{Sc}C_1' - n\mathrm{Sc}C_1 = -A\mathrm{Sc}C_0' - \mathrm{SoSc}\vartheta_1^{''}. \quad (27)$$

The corresponding boundary conditions can be written as:

– at $y = 0$

$$u_0 = U_p, \quad u_1 = 0, \quad \vartheta_0 = 1, \quad \vartheta_1 = 1, \quad C_0 = 1, \quad C_1 = 1, \quad (28)$$

– as $y \to \infty$

$$u_0 \to u_1 \to 1, \quad \vartheta_0 \to 0, \quad \vartheta_1 \to 0, \quad C_0 \to 0, \quad C_1 \to 0.$$

Finally, by solving Eqs. (22) to (27), we obtain analytical solutions in the form of Eqs. (29) to (34), which satisfy the above boundary conditions (28):

$$u_0 = 1 + J_1 e^{m_2 y} + J_2 e^{m_6 y} + J_3 e^{m_2 y} + J_4 e^{m_{10} y}, \quad (29)$$

$$u_1 = 1 + J_6 e^{m_{10} y} + J_7 e^{m_2 y} + J_8 e^{m_6 y} + J_9 e^{m_2 y} + \\ + J_{10} e^{m_4 y} + J_{11} e^{m_2 y} + J_{12} e^{m_8 y} + J_{13} e^{m_6 y} + \\ + J_{14} e^{m_2 y} + J_{15} e^{m_2 y} + J_{16} e^{m_4 y} + J_{17} e^{m_{12} y}, \quad (30)$$

$$\vartheta_0 = e^{m_2 y}, \quad (31)$$

$$\vartheta_1 = D_1 e^{m_2 y} + D_2 e^{m_4 y}, \quad (32)$$

$$C_0 = B_1 e^{m_2 y} + B_2 e^{m_6 y}, \quad (33)$$

$$C_1 = B_3 e^{m_6 y} + B_4 e^{m_2 y} + B_5 e^{m_6 y} + \\ + D_3 e^{m_2 y} + D_4 e^{m_4 y}. \quad (34)$$

The shapes of functions that appear in Eqs. (29)–(34) are explained in Appendix.

Distributions of velocity, temperature and concentration along with the boundary conditions, become visible in an overview of the aforementioned solutions:

$$u(y,t) = 1 + J_1 e^{m_2 y} + J_2 e^{m_6 y} + J_3 e^{m_2 y} + J_4 e^{m_{10} y} + \\ + \varepsilon e^{nt}(1 + J_6 e^{m_{10} y} + J_7 e^{m_2 y} + J_8 e^{m_6 y} + J_9 e^{m_2 y} + \\ + J_{10} e^{m_4 y} + J_{11} e^{m_2 y} + J_{12} e^{m_8 y} + J_{13} e^{m_6 y} + J_{14} e^{m_2 y} + \\ + J_{15} e^{m_2 y} + J_{16} e^{m_4 y} + J_{17} e^{m_{12} y}),$$

$$\vartheta(y,t) = e^{m_2 y} + \varepsilon e^{nt}(D_1 e^{m_2 y} + D_2 e^{m_4 y}),$$

$$C(y,t) = B_1 e^{m_2 y} + B_2 e^{m_6 y} + \varepsilon e^{nt}(B_3 e^{m_6 y} + B_4 e^{m_2 y} + \\ + B_5 e^{m_6 y} + D_3 e^{m_2 y} + D_4 e^{m_4 y}).$$

It is critical to compute the basic physical quantities of interest, which are the local surface heat and mass flux. Using the temperature field in the boundary layer, we can calculate the local surface heat flux, represented by the Nusselt number (Nu):

$$\mathrm{Nu} = \frac{q_w^*}{k(T_w^* - T_\infty^*)} \implies \mathrm{Nu}\,\mathrm{Re}_x = \left(1 + \frac{4R}{3}\right)\left(\frac{\partial \vartheta}{\partial y}\right)_{y=0} \\ = \left(1 + \frac{4R}{3}\right)[m_2 + \varepsilon e^{nt}(m_2 D_1 + m_4 D_2)],$$

where $\mathrm{Re}_x = \frac{V_0 L}{\nu}$.

For the mass flux, we can calculate:

$$\mathrm{Sh} = \left(\frac{\partial C}{\partial y}\right)_{y=0} = m_2 B_1 + m_6 B_2 + \\ + \varepsilon e^{nt}(m_6 B_3 + m_2 B_4 + m_8 B_5).$$

3. Results and discussion

Graphs are utilized in this section to visually present numerical outcomes, aiding in the comprehension of the underlying physical phenomena. The investigation primarily focuses on analyzing velocity, temperature and concentration profiles across a spectrum of parameter values. Figures 2–19 are specifically generated for this purpose. Within these figures, Fig. 2 elucidates the impact of the Grashof number (Gr) on velocity profiles. Gr represents the approximate ratio between thermal buoyancy and viscous forces exerted on a fluid; alterations in Gr lead to changes in buoyancy while concurrently influencing viscous forces. A reduction in fluid viscosity corresponds to a decrease in internal resistance, consequently resulting in an augmentation of fluid velocity.

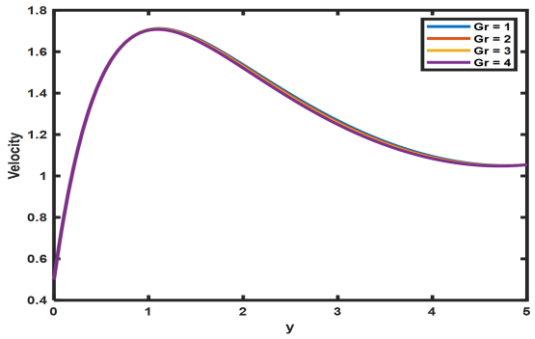

Fig. 2. Velocity profile for different values of Gr against *y*.

Figure 3 shows how the modified Grashof number (Gm) affects the velocity profiles. Gm is approximately the proportion of the buoyancy concentration to the viscous force acting on the fluid; a Gm increase leads to an enlarging buoyancy force while decreasing the viscous force. Viscosity is a type of internal resistance that occurs when a fluid is in motion. As the fluid's viscosity decreases, so does its internal resistance, increasing the velocity.

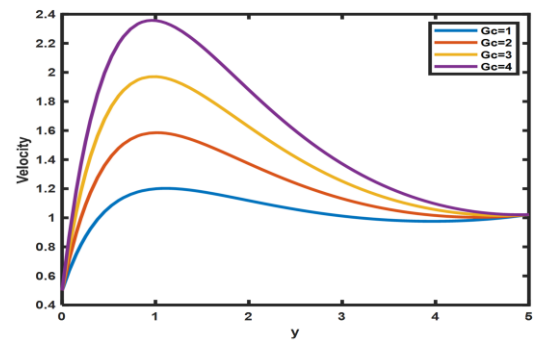

Fig. 3. Velocity profile for different values of Gm against *y*.

The velocity is depicted in Fig. 4 for various permeability values (N). It is self-evident that as permeability increases, so does the peak velocity. Due to the increase in permeability, there are more and larger pathways available for fluid flow within the porous medium, this allows for greater fluid movement and higher velocities. Higher permeability reduces the pressure drop across the porous medium for a given flow rate. With less pressure drop, there is less resistance to flow, enabling the fluid to move more freely and at high velocities.

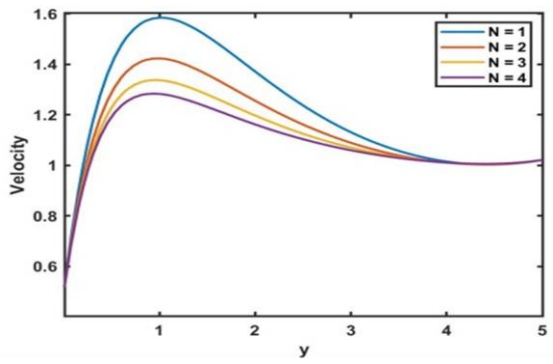

Fig. 4. Velocity profile for different values of N against y.

The modifications of velocity profiles with the Prandtl number Pr are shown in Fig. 5. This explains the motion of fluid which slows the resultant velocity because of the rise in Pr. The Prandtl number is the relationship between two diffusions, momentum and thermal, and is described as the ratio of momentum diffusion and thermal diffusion. Enhancing the Prandtl number reduces the thermal diffusion, causing the thermal boundary layer to thin. As a result, Pr increases across the fluid's occupied region, and the resultant velocity decreases. It is reasonable because the fluid has a large Prandtl number and a greater viscosity due to its thickness.

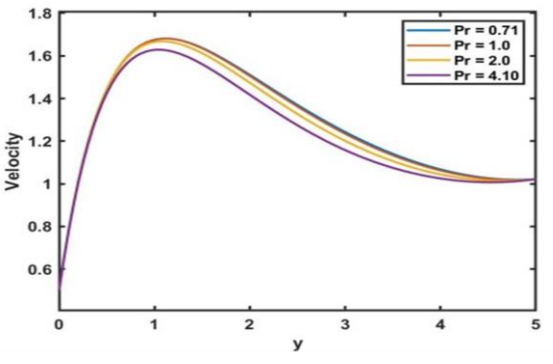

Fig. 5. Velocity profile for different values of Pr against y.

Figure 6 depicts the Soret number (So), which is observed to affect velocity profiles. This figure shows that as So increases, the velocity profiles increase, implying that the velocity of the fluid increases due to larger thermal diffusion. The effect of thermal diffusion is visible in this figure, as the fluid flow is accelerated.

The velocity profile with Schmidt number (Sc) values is depicted in Fig. 7. The velocity distribution will usually decrease as the Schmidt number increases. In terms of physics, a higher Schmidt number indicates a lower molecular diffusivity, resulting in a thinner momentum boundary layer. A decrease in velocity distribution with the increasing Sc number may be associated

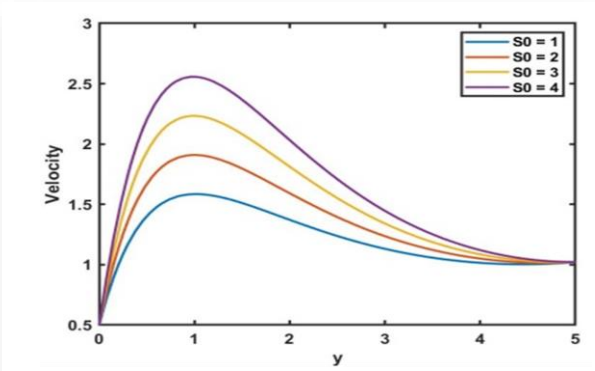

Fig. 6. Velocity profile for different values of So against y.

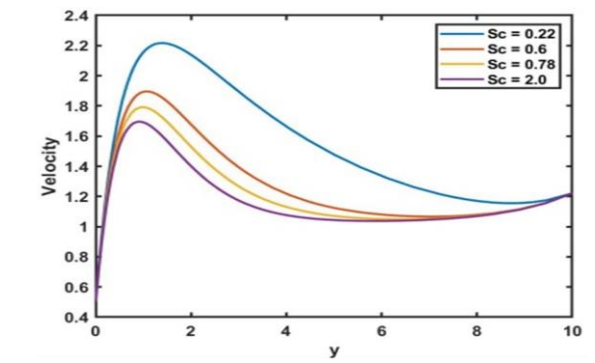

Fig. 7. Velocity profile for different values of Sc against y.

with increased flow stability. The slower diffusion of mass can lead to more stable concentration profiles, which in turn can lead to more uniform flow and reduced velocity gradients.

Figures 8 and 12 illustrate the impact of the heat source (Q) on velocity and concentration profiles. Figures 8 and 12 demonstrate that as heat is produced, the buoyancy force enhances, as a result of which the velocity curves coincide and the flow rate increases, resulting in concentration profiles. The deviation of velocity distribution concerning the thermal radiation R, is shown in Fig. 9. This shows that as thermal radiation enlarges, the velocity within the boundary layer increases. The momentum boundary layer thickness rises in proportion to the increase in thermal radiation. Temperature profiles for various heat source parameter (Q) settings are shown in Fig. 10. As shown in Fig. 10, increasing the heat source parameters reduces the temperature profiles. As the heat source parameters increase, there is more thermal energy available to dissipate throughout the system. This increased energy availability results in more efficient heat dissipation, leading to lower temperature gradients and reduced temperature profiles.

Figure 11 depicts the effect of Prandtl number (Pr) on temperature profiles. The Prandtl number is approximately the ratio of the kinematic viscosity and thermal diffusivity. Higher Prandtl values can aid in the reduction of thermal diffusiveness, which leads to a decrease in temperature profiles. It is clear from Fig. 13 that as the thermal radiation (N) is increased, the concen-

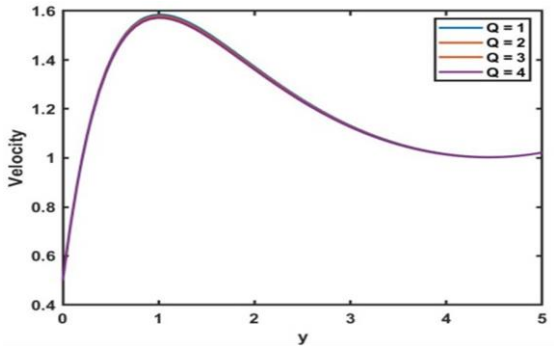

Fig. 8. Velocity profile for different values of Q against y.

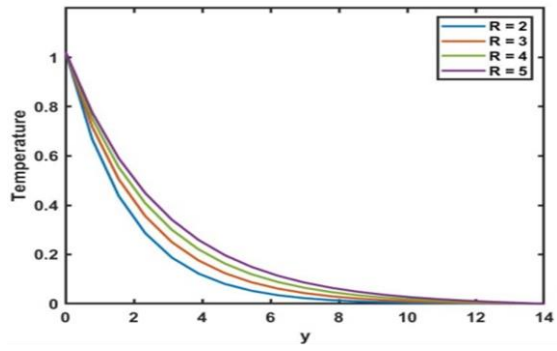

Fig. 9. Temperature profile for different values of R against y.

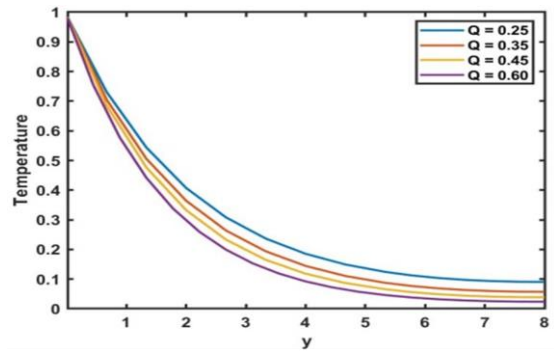

Fig. 10. Temperature profile for different values of Q against y.

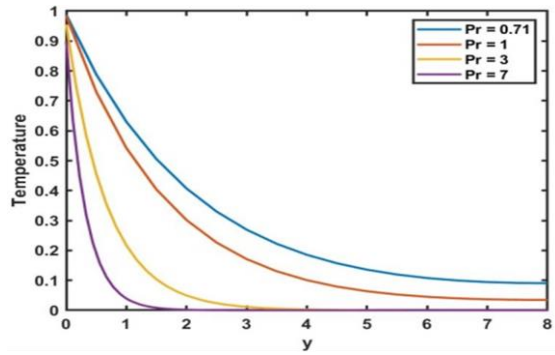

Fig. 11. Temperature profile for different values of Pr against y.

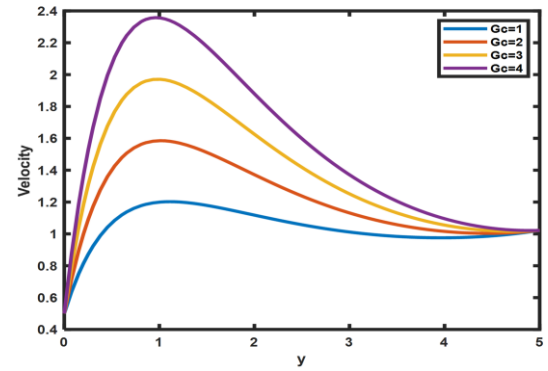

Fig. 12. Concentration profile for different values of Q against y.

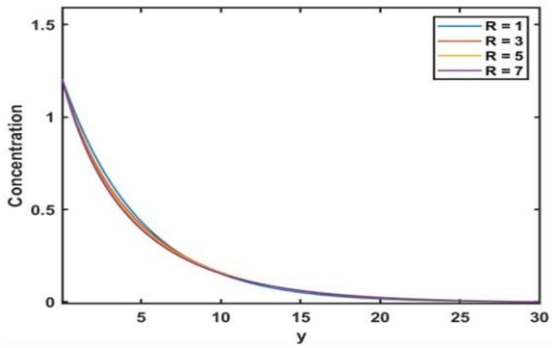

Fig. 13. Concentration profile for different values of R against y.

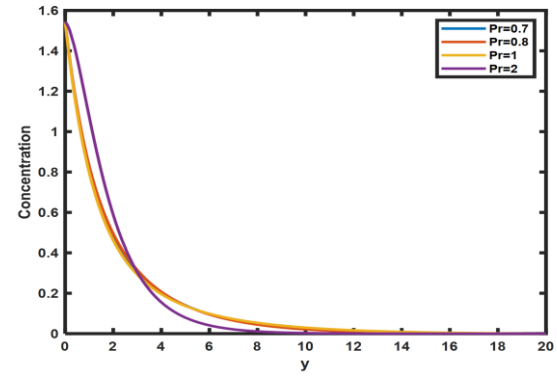

Fig. 14. Concentration profile for different values of Pr against y.

tration decreases. Higher N values cause the fluid concentration to be delayed. Similarly, for the concentration distribution: with the increasing Pr number, the boundary layer thickness shrinks, which is shown in Fig. 14.

Figure 15 illustrates the influence of the Schmidt number (Sc) on concentration profiles. It is observed that higher Sc values, representing lower diffusivity, lead to a reduction in concentration throughout the flow region. An increase in Sc correlates with reduced solute diffusivity, limiting the dispersion of solute effects. Consequently, while the concentration within the flow region increases, the boundary layer thickness decreases, resulting in an overall reduction in concentration as Sc rises. The Soret effect is a phenomenon that occurs when the concentration distribution is influenced by a temperature gradient. In physical

terms, higher Soret numbers indicate a more pronounced temperature gradient, leading to increased convective flow. Consequently, the concentration distribution expands, as illustrated in Fig. 16.

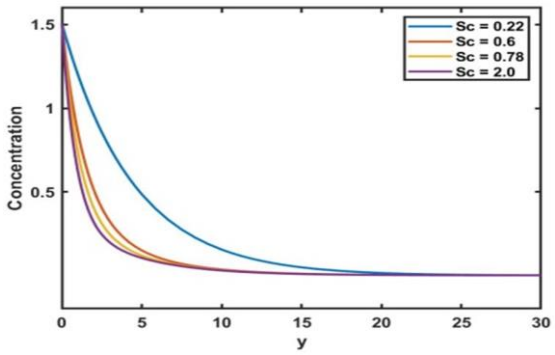

Fig. 15. Concentration profile for different values of Sc against *y*.

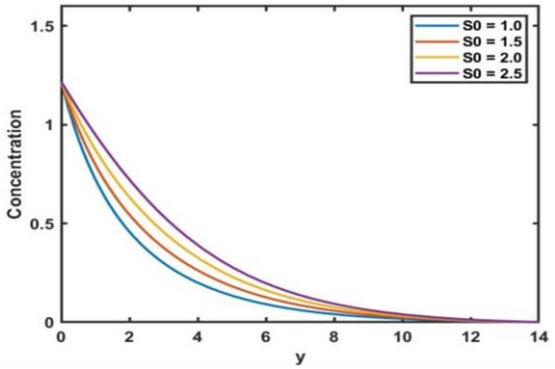

Fig. 16. Concentration profile for different values of So against *y*.

Figure 17 illustrates the influence of radiation (R) on the heat transfer rate, represented by the Nusselt number (Nu). As the radiation parameter enlarges, the rate of heat transfer (Nu) decreases. This reduction occurs because increasing the radiation parameter can diminish the effectiveness of convective heat transfer. Radiation heat transfer tends to suppress convective heat transfer, especially in regions where radiation predominates. Consequently, an increase in the radiation parameter may lead to a decrease in the convective heat transfer coefficient, resulting in lower overall heat transfer rates.

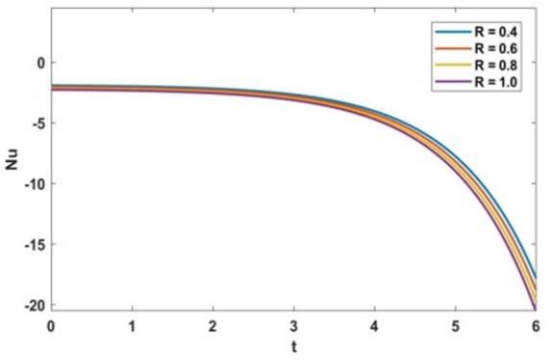

Fig. 17. Nusselt number profile for different values of *R* against *t*.

Figure 18 showcases the effect of the Soret number (So) on the Sherwood number (Sh) on the porous plate. The findings demonstrate that augmenting the value of So leads to an increase in the Sherwood number, indicating enhanced mass transfer rates.

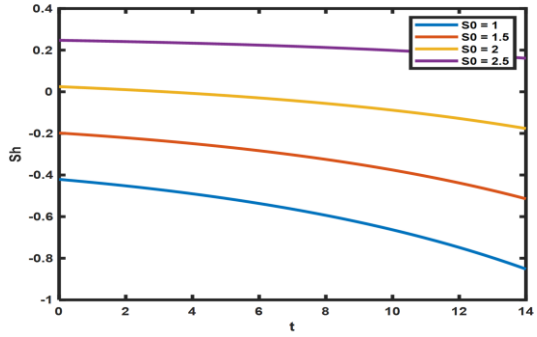

Fig. 18. Sherwood number for different values of So against *t*.

Figure 19 depicts the impact of rotation parameters on fluid velocity. Increasing the rotation parameter decreases the fluid velocity. With a gradual increase in rotation, the fluid's velocity closely adheres to the boundary and gradually diminishes as the distance from the boundary increases.

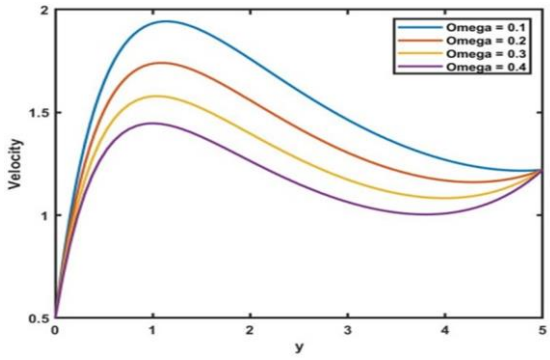

Fig. 19. Velocity profile for different values of Ω against *y*.

4. Conclusions

The main focus of this study revolves around examining the influence of rotation on the magnetohydrodynamic unsteady heat and mass transfer flow of a convective, viscous fluid through a porous medium past a vertically moving plate. The governing equations are solved using the perturbation technique. The resulting profiles, including the temperature, velocity and concentration, are graphically presented and extensively discussed for various parameter configurations. The principal discoveries of this investigation are as follows:

– The velocity increases as Gr, Gm, N, and So increase. Whereas the velocity decreases as the Pr, M, and Sc increase. The velocity profiles are unaffected by the heat source parameter (Q). The heat source parameter represents an external heat input into the system, such as thermal

radiation. This heat input affects the temperature distribution within the fluid but does not directly exert a force on the fluid particles to change their velocity. Therefore, variations in the heat source parameter do not directly alter the velocity profile;

- The temperature increases as radiation enhances, while the temperature decreases as Pr and *Q* increase;
- The rotation is increased gradually, and the fluid's velocity follows the boundary and is trivially far away from it. As the system rotates, the fluid near the boundary experiences a centrifugal force directed away from the axis of rotation. This centrifugal force causes the fluid to move tangentially along the boundary, following its curvature. The fluid velocity along the boundary tends to be higher compared to the fluid velocity in the interior of the flow domain due to the influence of the rotating motion;
- The Nu number reduces as *R* enlarges, while the Sh number enhances as the So number increases.

Appendix

In this Appendix, functions that appear in Eqs. (29)–(34) are explained below:

$$\beta_1 = \left(\frac{3+4R}{3\mathrm{Pr}}\right),$$

$$m_2 = \left(\frac{-1+\sqrt{1+4Q\beta_1}}{2\beta_1}\right),$$

$$m_4 = \left(\frac{-1+\sqrt{1+4(n+Q)\beta_1}}{2\beta_1}\right),$$

$$m_6 = -\mathrm{Sc},$$

$$m_8 = \left(\frac{-\mathrm{Sc}+\sqrt{(\mathrm{Sc})^2+4n\mathrm{Sc}}}{2}\right),$$

$$m_{10} = \left(\frac{-1+\sqrt{1-4(2\Omega-N)}}{2}\right),$$

$$m_{12} = \left(\frac{-1+\sqrt{1+4(N+n+2\Omega)}}{2}\right),$$

$$J_1 = -\left(\frac{\mathrm{Gr}}{m_2^2+m_2+(2\Omega-N)}\right),$$

$$J_2 = -\left(\frac{\mathrm{Gm}B_1}{m_6^2+m_6+(2\Omega-N)}\right),$$

$$J_3 = -\left(\frac{\mathrm{Gm}B_2}{m_{10}^2+m_{10}+(2\Omega-N)}\right),$$

$$J_4 = (U_p - 1 - J_1 - J_2 - J_3),$$

$$J_6 = -\left(\frac{AJ_4m_{10}}{m_{10}^2+m_{10}-(N+n+2\Omega)}\right),$$

$$J_7 = -\left(\frac{AJ_1m_2}{m_2^2+m_2-(N+n+2\Omega)}\right),$$

$$J_8 = -\left(\frac{AJ_3m_6}{m_6^2+m_6-(N+n+2\Omega)}\right),$$

$$J_9 = -\left(\frac{AJ_2m_2}{m_2^2+m_2-(N+n+2\Omega)}\right),$$

$$J_{10} = -\left(\frac{\mathrm{Gr}D_2}{m_4^2+m_4-(N+n+2\Omega)}\right),$$

$$J_{11} = -\left(\frac{\mathrm{Gr}D_1}{m_2^2+m_2-(N+n+2\Omega)}\right),$$

$$J_{12} = -\left(\frac{\mathrm{Gm}B_5}{m_2^2+m_2-(N+n+2\Omega)}\right),$$

$$J_{13} = -\left(\frac{\mathrm{Gm}B_2}{m_6^2+m_6-(N+n+2\Omega)}\right),$$

$$J_{14} = -\left(\frac{\mathrm{Gm}B_4}{m_2^2+m_2-(N+n+2\Omega)}\right),$$

$$J_{15} = -\left(\frac{\mathrm{Gm}D_3}{m_2^2+m_2-(N+n+2\Omega)}\right),$$

$$J_{16} = -\left(\frac{\mathrm{Gm}D_4}{m_4^2+m_4-(N+n+2\Omega)}\right),$$

$$J_{17} = -\left(\begin{matrix}1+J_7+J_8+J_9+J_6+J_{11}+J_{10}+\\+J_{13}+J_{14}+J_{12}+J_{15}+J_{16}\end{matrix}\right),$$

$$D_1 = -\left(\frac{Am_2}{\beta_1 m_2^2+m_2-(n+Q)}\right),$$

$$D_2 = (1 - D_1),$$

$$D_3 = -\left(\frac{\mathrm{ScSo}m_2^2D_1}{m_2^2+\mathrm{Sc}m_2-n\mathrm{Sc}}\right),$$

$$D_4 = -\left(\frac{\mathrm{ScSo}m_4^2D_2}{m_4^2+\mathrm{Sc}m_4-n\mathrm{Sc}}\right),$$

$$B_1 = \frac{-\mathrm{Sc}\,\mathrm{So}m_2}{m_2+\mathrm{Sc}},$$

$$B_2 = (1 - B_1),$$

$$B_3 = -\left(\frac{A\mathrm{Sc}m_6B_2}{m_6^2+\mathrm{Sc}m_6-n\mathrm{Sc}}\right),$$

$$B_4 = -\left(\frac{A\mathrm{Sc}m_2B_1}{m_2^2+\mathrm{Sc}m_2-n\mathrm{Sc}}\right),$$

$$B_5 = (1 - B_3 - B_4 - D_3 - D_4).$$

References

[1] Chamkha, A., Mansour, M.A., & Aly, A. (2011), Unsteady MHD free convective heat and mass transfer from the vertical porous plate with Hall current, thermal radiation and chemical reaction effects. *International Journal for Numerical Methods in Fluids*, 65(4), 432−447. doi: 10.1002/fld.2190

[2] Mohyud–Din, S.T., Khan, U., Ahmed, N., & Rashidi, M.M. (2018). A Study of heat and mass transfer on Magnetohydrodynamic (MHD) flow of nanoparticles. *Propulsion and Power Research*, 7(1), 72–77. doi: 10.1016/j.jppr.2018.02.001

[3] Kataria, H., & Patel, H. (2018), Heat and mass transfer in Magnetohydrodynamic (MHD) Casson fluid flow past over an oscillating vertical plate embedded in a porous medium with ramped wall temperature. *Propulsion and Power Research*, 7(3), 257−267. doi: 10.1016/j.jppr.2018.07.003

[4] Seth, G.S., Sarkar, S., & Hussain, S.M. (2014). Effects of Hall current radiation and rotation on natural convection heat and mass transfer flow past a moving vertical plate. *Ain Shams Engineering Journal*, 5(2), 489−503. doi: 10.1016/j.asej.2013.09.014

[5] Seth, G.S., Hussain, S.M., & Sarkar S. (2014). Effects of Hall current and rotation on unsteady MHD natural convection flow

with heat and mass transfer past an impulsively moving vertical plate in the presence of radiation and chemical reaction. *Bulgarian Chemical Communications,* 46(4), 704−718.

[6] Shevchuk, I.V. (2016). *Modelling of Convective Heat and Mass Transfer in Rotating Flows*. Mathematical Engineering, Springer International Publishing. doi: 10.1007/978-3-319-20961-6

[7] Takhar, H.S., Singh, A.K, & Nath. G. (2002). Unsteady MHD flow and heat transfer on a rotating disk in an ambient fluid. *International Journal of Thermal Sciences*, 41(2), 147−155. doi: 10.1016/S1290-0729(01)01292-3

[8] Jha, B.K., & Apere, C.A. (2010), Combined effect of Hall and ion-slip currents on unsteady MHD Couette flow in a rotating system. *Journal of the Society of Japan*, 79(10), 104401. doi: 10.1143/ JPSJ.79.104401

[9] Abdel Rahman, G.M. (2008), Thermal Diffusion and MHD effects on combined free forced convection and mass transfer of a viscous fluid flow through a porous medium with heat generation. *Chemical Engineering and Technology*, 31(4), 554-559. doi: 10.1002/ceat.200700487

[10] Veera Krishna, M., Ameer Ahamad, N., & Chamkha, A.J. (2020), Hall and ion slip effects on unsteady MHD free convective rotating flow through a saturated porous medium over an exponential plate. *Alexandria Engineering Journal*, 59(2), 565−577. doi: 10.1016/j.aej.2020.01.043

[11] Ahmmed, S.F., Das, M.K., & Ali, L.E. (2015). Analytical study on unsteady MHD free convection and mass transfer flow past a vertical porous plate. *American Journal of Applied Mathematics*, 3(2), 64−74. doi: 10.11648/j.ajam.20150302.16

[12] Seddeek, M.A. (2002). Effects of radiation and variable viscosity on a MHD free convection flow past a semi-infinite flat plate with an aligned magnetic field in the case of unsteady flow. *International Journal of Heat Mass Transfer*, 45(4), 931−935. doi: 10.1016/S0017-9310(01)00189-2

[13] Niveditha, P. & Prasad, B.V.S.S.S. (2021). Computational Analysis on the Performance of Centrifugal Compressor with Tapered Wall and Rotating Tapered Wall Vaneless Diffuser. *Journal of Applied Fluid Mechanics*, 14(2), 641–656. doi: 10.47176/jafm.14.02.32008

[14] Anirudh Narayanan, B., Lakshmanan, G., Mohammad, A. & Ratna Kishore V. (2021). Laminar Flow over a Square Cylinder Undergoing Combined Rotational and Transverse Oscillations. *Journal of Applied Fluid Mechanics*, 14(1), 259-273. doi: 10.47176/jafm.14.01.30706

[15] Rudziva, M., Sibanda, P., Noreldin, O.A.I., & Goqo, S.P. (2022). A Numerical study of heat and mass transfer in a Darcy porous medium saturated with a couple of stress fluid under rotational modulation. *Applied Mathematical Modelling*, 104, 455–473. doi: 10.1016/j.apm.2021.12.004